

Observation of Aharonov-Bohm effect in PbTe nanowire networks

Zuhan Geng,^{1,*} Zitong Zhang,^{1,*} Fangting Chen,^{1,*} Shuai Yang,^{1,2} Yuying Jiang,¹ Yichun Gao,¹ Bingbing Tong,² Wenyu Song,¹ Wentao Miao,¹ Ruidong Li,¹ Yuhao Wang,¹ Qinghua Zhang,³ Fanqi Meng,³ Lin Gu,³ Kejing Zhu,² Yunyi Zang,² Lin Li,² Runan Shang,² Xiao Feng,^{1,2,4} Qi-Kun Xue,^{1,2,4,5} Ke He,^{1,2,4,†} and Hao Zhang^{1,2,4,‡}


¹State Key Laboratory of Low Dimensional Quantum Physics, Department of Physics, Tsinghua University, Beijing 100084, China

²Beijing Academy of Quantum Information Sciences, Beijing 100193, China

³Institute of Physics, Chinese Academy of Sciences, Beijing 100190, China

⁴Frontier Science Center for Quantum Information, Beijing 100084, China

⁵Southern University of Science and Technology, Shenzhen 518055, China

 (Received 23 December 2021; revised 13 February 2022; accepted 13 June 2022; published 22 June 2022)

We report phase coherent electron transport in PbTe nanowire networks with a loop geometry. Magnetoconductance shows Aharonov-Bohm (AB) oscillations with periods of h/e and $h/2e$ in flux. The amplitudes of $h/2e$ oscillations are enhanced near zero magnetic field, possibly due to interference between time-reversal paths. Temperature dependence of the AB amplitudes suggests a phase coherence length $\sim 8\text{--}12\ \mu\text{m}$ at 50 mK. This length scale is larger than the typical geometry of PbTe-based hybrid semiconductor-superconductor nanowire devices.

DOI: [10.1103/PhysRevB.105.L241112](https://doi.org/10.1103/PhysRevB.105.L241112)

Topological quantum computing relies on braiding of Majorana zero modes (MZMs) to realize various quantum gate operations [1,2]. A major theoretical proposal is the so-called measurement-based braiding where the topological qubit can be readout from interference between a MZM-involved path (electron “teleportation”) and a normal (topologically trivial) path [3–6]. Therefore, phase coherent transport is a crucial ingredient along this roadmap. A one-dimensional (1D) semiconductor-superconductor hybrid nanowire is a promising MZM candidate [7–10] where the phase coherent transport can be revealed as Aharonov-Bohm (AB) oscillations in nanowire networks with a loop geometry. Among all 1D candidates, InSb and InAs nanowires are the most studied MZM material systems [11–17], with AB effect demonstrated [18–21]. Recently, PbTe [22–27] based nanowires [28,29] have been proposed as a new MZM candidate [30]. In this paper, we report the observation of AB effect in PbTe nanowire networks.

Figure 1(a) (inset) shows the scanning electron micrograph (SEM) of a PbTe nanowire, selectively grown on a CdTe substrate using molecular beam epitaxy (MBE). The nanowire is contacted by two normal metal leads (yellow, Ti/Au) and then covered by a layer of HfO₂ dielectric with a Ti/Au top gate (TG). The selective area growth (SAG) of PbTe is achieved by covering the CdTe substrate with an Al₂O₃ dielectric mask followed by wet etching for trenches. Growth details can be found in our recent work [29] where a CdTe(001) substrate was used. In this work we choose a different substrate orientation, CdTe(111), for the PbTe growth. Valley degeneracy

breaking along this (111) direction, which is crucial in the realization of MZMs, has been experimentally demonstrated [25,27] and theoretically verified [30].

Fitting the pinch-off curve (for the upward sweeping direction) of this field effect device [Fig. 1(a)] suggests a mobility $\sim 0.94 \times 10^4\ \text{cm}^2/\text{V s}$. The mobility extracted from the downward sweeping is roughly halved, see Fig. S1 in Ref. [31] for details. For detailed discussion of PbTe hysteresis and mobility, we refer to our previous work [29]. The capacitance (C) is estimated using a finite element model based on the device cross section. Figure 1(b) shows the low-magnification cross-sectional high-angle annular dark-field (HAADF) image of the device. The top PbTe surface is capped with CdTe, preventing possible oxidation. This capping may enhance the device mobility and coherence length. Clearly the cross section of the PbTe bottom has an irregular shape with rough interfaces, possibly due to the Ar treatment of the CdTe substrate before the PbTe growth. This interface can be a major source of disorder [32–36] and future growth optimization for flat interface may lead to higher mobility. Nevertheless, magnification of the interface can still resolve matched lattices between PbTe and CdTe, see Fig. 1(c) for the enlarged HAADF. So far we have not found stacking faults/defects based on the cross sectional TEM. We speculate that the matched lattice between PbTe nanowire and CdTe substrate (even being rough) could prevent the heterostructure from having stacking faults.

Figure 1(d) shows the SEM and three-dimensional (3D) schematic of a PbTe network device (device A), grown and fabricated (contact, dielectric, and gate) together with the mobility device on the same substrate chip. The voltage applied to the top gate (V_{TG}) tunes the carrier density in the nanowire loop. To ensure ohmic contact, the CdTe layer was etched by Ar plasma before the Ti/Au deposition. Scanning

*These authors contributed equally to this paper.

[†]kehe@tsinghua.edu.cn

[‡]hzquantum@mail.tsinghua.edu.cn

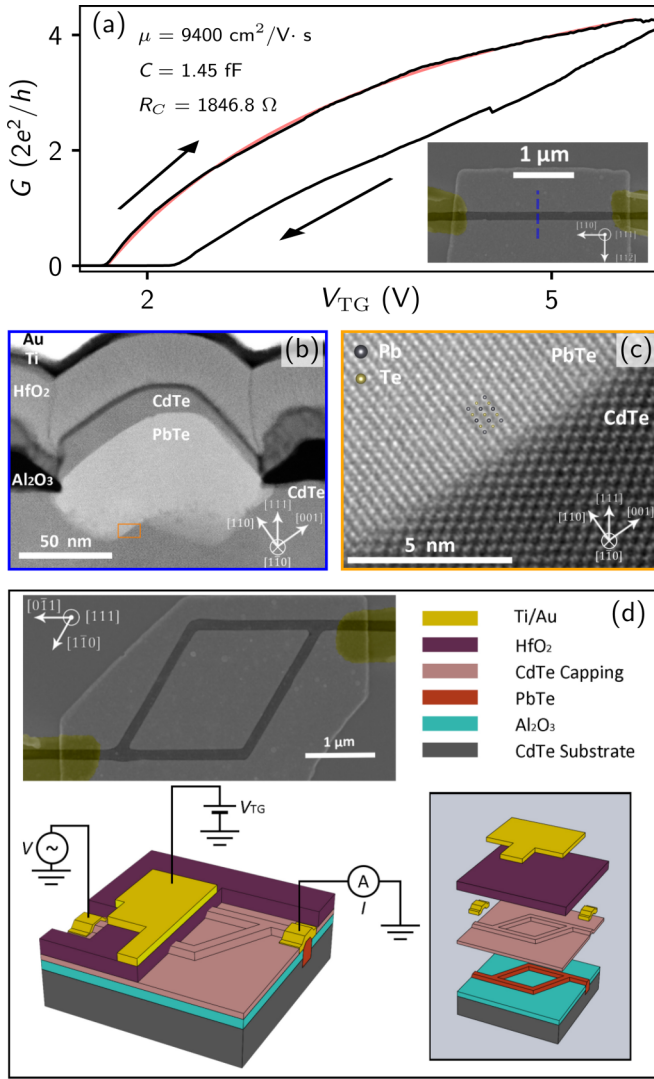


FIG. 1. (a) Pinch-off of a PbTe nanowire with the mobility fit (red line). Inset: Device SEM. (b) Cross-sectional HAADF with crystal directions labeled. (c) Enlarged HAADF of the orange box in (b). (d) SEM of device A (nanowire loop) and its 3D schematic.

transmission electron microscope (STEM) of device A can be found in Fig. S2 in Ref. [31].

Figure 2(a) shows the magnetoconductance of device A, measured in a dilution refrigerator with a base temperature ~ 20 mK. The differential conductance G was measured using a lock-in amplifier in a two terminal circuit setup. The bias voltage was fixed at zero throughout the measurement. The magnetic field (B) was oriented perpendicular to the substrate for Fig. 2(a). The overall conductance shows a peak near $B = 0$ T, suggesting the existence of weak antilocalization (WAL). On top of the background, periodic AB oscillations are resolved with periods of $\Delta B \sim 1.4$ mT (orange inset) and ~ 0.7 mT (red inset), corresponding to flux periods of h/e (first harmonic) and $h/2e$ (second harmonic), respectively. Here h is the Planck constant and e is the electron charge. The $h/2e$ -AB oscillations are also known as Altshuler-Aronov-Spivak (AAS) effect [37,38]. We further convert this period in ΔB into an effective loop area $A \sim 2.95 \mu\text{m}^2$ based on the formula

of $\Delta B \times A = h/e$. This extracted area is close to the area defined by the inner surface of the nanowire loop $\sim 2.9 \mu\text{m}^2$ (the area of the outer loop is $\sim 3.92 \mu\text{m}^2$), suggesting that the electron wave function is mainly distributed near the inner surface.

For a control test we also apply B parallel to the substrate and observe a WAL peak without AB oscillations [Fig. 2(b)]. In Fig. 2(c) we plot the spectrum of fast Fourier transform (FFT) where the h/e and $h/2e$ oscillations in Fig. 2(a) are revealed as two FFT peaks (see the black curve). By contrast, the FFT of Fig. 2(b) shows no such peaks [the red curve in Fig. 2(c)]. Boundaries of the shaded area refer to the expected h/e AB periods, estimated based on the area encircled by the inner and outer surfaces of the nanowire loop. The dashed line is the expected peak position of the second harmonic ($h/2e$), calculated by multiplying the center of the first harmonic peak by a factor of 2.

We further show the magnetoconductance of device A at different gate voltages (see Fig. S3 in Ref. [31]). The AB amplitude varies for different gate voltages, as well as for the same gate voltage but repeated measurements, possibly due to device instabilities. In some gate settings we observe no AB oscillations, possibility due to the pinch-off of one of the two AB “arms” or other unknown dephasing mechanisms, see Fig. S4 in Ref. [31] for the statistics. Figure 2(d) shows examples for h/e and $h/2e$ oscillations with amplitudes reaching ~ 0.015 and 0.02 , in the unit of $2e^2/h$. In Fig. 2(e) we show the ensemble averaged FFT for all (in total 182 sets) measured B -sweeping curves (the black line), where the first and second harmonic peaks are clearly visible. The second harmonic peak has a similar height as the first one, suggesting a significant $h/2e$ component. The $h/2e$ oscillations in Fig. 2(a) are mostly prominent near $B = 0$ T, possibly due to the time-reversal paths. To confirm this hypothesis, we perform the ensemble averaged FFT for B near 0 T [blue curve in Fig. 2(e)] which indeed resolves a more prominent $h/2e$ peak. By contrast, the averaged FFT for higher B resolves a much smaller $h/2e$ peak [red curve in Fig. 2(e)]. In addition, in Fig. 2(f) with a small fixed in-plane magnetic field of 30 mT, the out-of-plane magnetoconductance reveals mainly the h/e oscillations even for out-of-plane B near 0 T. The corresponding FFT [Fig. 2(g)] also confirms that the $h/2e$ peak is hardly visible.

We now study the temperature dependence of the AB oscillations. Figure 3(a) shows the h/e oscillations with the temperature varies from 21 to 780 mK (only six curves are shown for clarity). The T evolution of AB amplitudes is more visible after subtracting an overall background (by smoothing the curve), as shown in Fig. 3(b) which focuses on the B ranges with large oscillations. The oscillation amplitude is reduced by roughly half at $T \sim 200$ – 300 mK, and almost vanishes at $T \sim 510$ mK. Figure 3(c) shows the $h/2e$ oscillations (background subtracted) at three typical T s, resolving a similar trend.

To quantify the h/e and $h/2e$ oscillation amplitudes, we perform FFT and estimate the amplitude by the “area” underneath the corresponding FFT peak. This area is calculated by numerical integration, see Fig. S5 in Ref. [31] for detailed information. Figure 3(d) shows h/e (left) and $h/2e$ (right) amplitudes, decaying with increasing T as a general trend. The fluctuations are possibly due to instabilities within the mesoscopic environment. To fit this decay, we adopt a

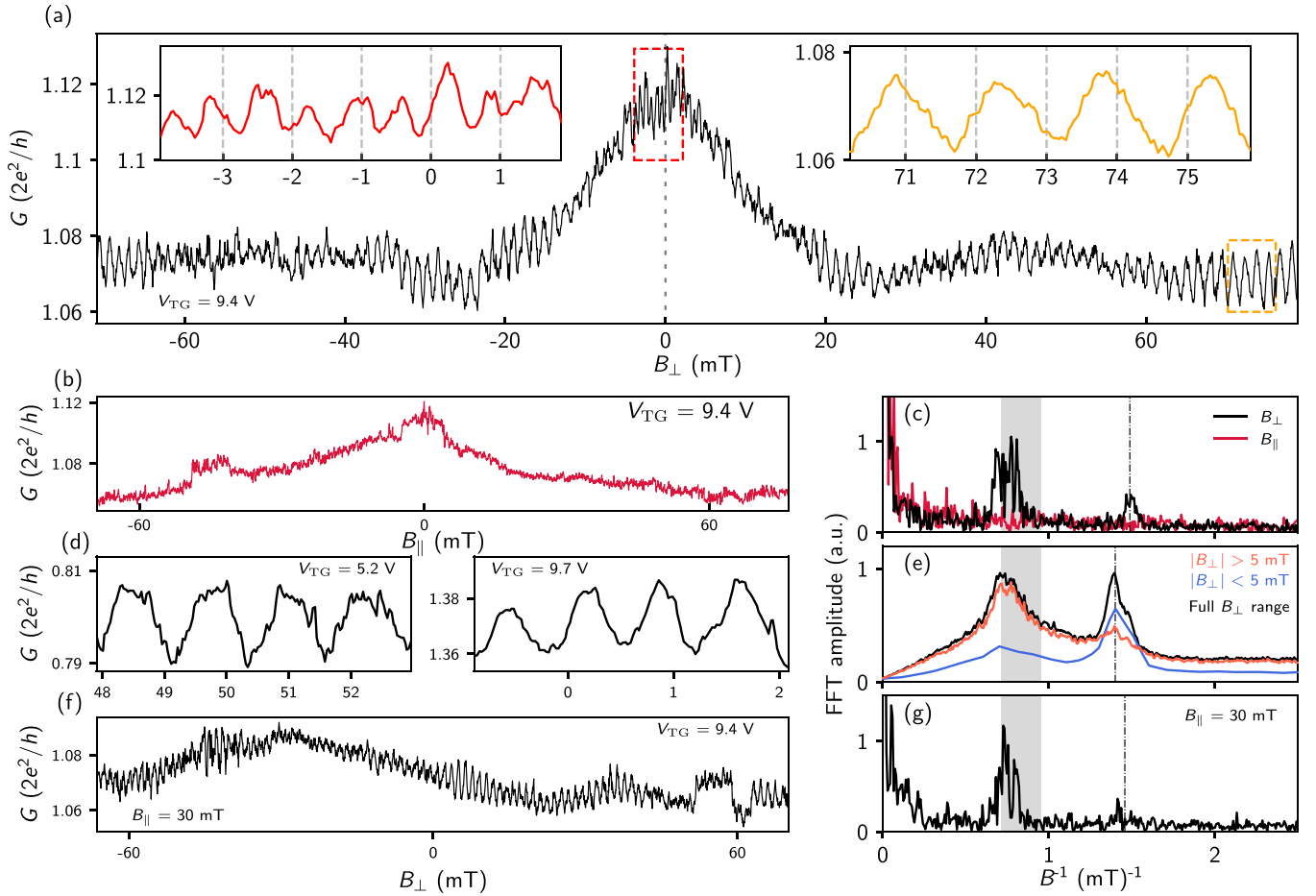


FIG. 2. AB oscillations in device A. (a) Magnetoconductance, B perpendicular to the substrate. Insets: Magnifications of the regions of $h/2e$ and h/e oscillations. (b) Magnetoconductance, B parallel to the substrate. B is offset by 4 and 2 mT for (a) and (b), based on the symmetry of the WAL. (c) FFT of (a) (black) and (b) (red). (d) Two more AB curves, B perpendicular to the substrate. (e) Black: Ensemble averaged FFT, after subtracting a conductance background (smooth window 1.42 mT). Blue: Ensemble averaged FFT by limiting the B range below 5 mT. Red: Averaged FFT outside this range. (f) AB at a fixed in-plane B of 30 mT. (g) FFT of (f). In (c), (e), and (g), boundaries of the shaded area are the geometric bounds estimated from the device SEM. $T \sim 20$ mK.

diffusive transport model [20,39], where the AB amplitude is assumed to be $\propto e^{-L/L_\phi}$ and L_ϕ is assumed to be $\propto 1/\sqrt{T}$. L_ϕ is the phase coherence length and L is one half of the loop circumference for h/e and the full circumference for $h/2e$ oscillations. The fitting result [red lines in Fig. 3(d)] suggests a phase coherence length $L_\phi \sim 8\text{--}12 \mu\text{m}$ at a temperature of 50 mK. The error bar of L_ϕ is $2 \mu\text{m}$ for h/e and $1 \mu\text{m}$ for $h/2e$ oscillations, due to the sizable fluctuations (outliers). We note that the extracted L_ϕ value is only a rough estimation which may vary for different models. The extracted length scale (a few microns) is consistent with the observation of $h/2e$ oscillations: electrons remain phase coherent after circulating the whole loop which is $\sim 8 \mu\text{m}$.

Finally, we show AB oscillations observed in a second device (device B), also selectively grown on a CdTe(111) substrate. The loop geometry has a square shape instead of a diamond as shown in Figs. 4(a) and 4(b). The magnetoconductance [Fig. 4(c)] resolves AB oscillations with $h/2e$ period near zero B and h/e period at higher B , see Figs. 4(d) and 4(e) for the magnifications with corresponding colors. The AB periods for h/e and $h/2e$ oscillations are ~ 1.25 and 0.66 mT,

respectively. This period in B can be converted into an effective loop area of $\sim 3.3 \mu\text{m}^2$. Based on the device SEM, we can independently estimate the loop area to be ~ 3 and $4 \mu\text{m}^2$ for the inner and outer surfaces, respectively. Comparing with the evaluated loop area again suggests that the electrons are mainly located near the inner surface of the loop.

Figure 4(g) shows the FFT of Fig. 4(c), resolving the two harmonic peaks (the black curve). As a comparison, FFT of a B -scan curve (not shown), measured under the same gate voltage but with B parallel to the substrate, resolves no such peaks (the red curve). The $h/2e$ oscillations are also enhanced near zero B , similar to the case in device A. This $h/2e$ component can be reduced by a fixed in-plane B of 10 mT, as shown in Fig. 4(f). The corresponding FFT (for the whole range) also only resolves the h/e peak [Fig. 4(h)].

Due to the device instabilities, we have only performed temperature dependence for the $h/2e$ oscillations, see Fig. 4(i) for the oscillations at three different temperatures. In Fig. 4(j) we plot the FFT amplitude vs temperature, fit the diffusive transport model, and extract the phase coherence length $L_\phi = 9 \pm 2 \mu\text{m}$ at $T = 50$ mK. This result is roughly consistent

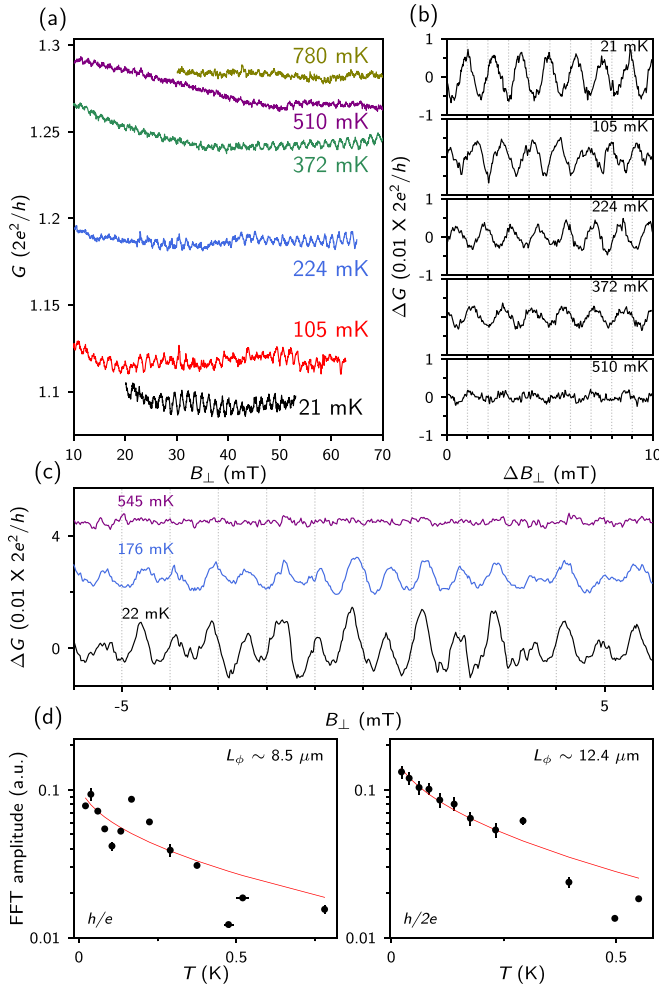


FIG. 3. Temperature (T) dependence of AB oscillations in device A. (a) h/e oscillations at several T s. $V_{TG} = 9.4$ V. (b) AB after subtracting a background (smooth window 1.42 mT). (c) $h/2e$ oscillations (background subtracted) at three T s. Vertical offsets are 0.025 and 0.045 ($\times 2e^2/h$) for clarity. $V_{TG} = 9.8$ V. (d) T dependence of the h/e (left) and $h/2e$ (right) FFT amplitudes for all measured T s. Red lines are fittings to extract the phase coherence length.

with the value of device A. For more B scans of device B, see Fig. S3 in Ref. [31].

To summarize, we have demonstrated phase coherent transport in PbTe nanowire networks by observing Aharonov-Bohm oscillations in magnetoconductance. Both h/e - and $h/2e$ -periodic oscillations can be revealed. Temperature dependence of the AB amplitude suggests a phase coherence length ~ 8 – 12 μm at $T = 50$ mK. This length scale exceeds the dimension of future PbTe-based hybrid semiconductor-superconductor devices, fulfilling a necessary condition for the exploration of topological quantum information processing. Future works could be aiming at the optimization of the nanowire growth for more uniform cross sections which may lead to higher mobility and longer phase coherence length.

Raw data and processing codes within this paper are available at [40].

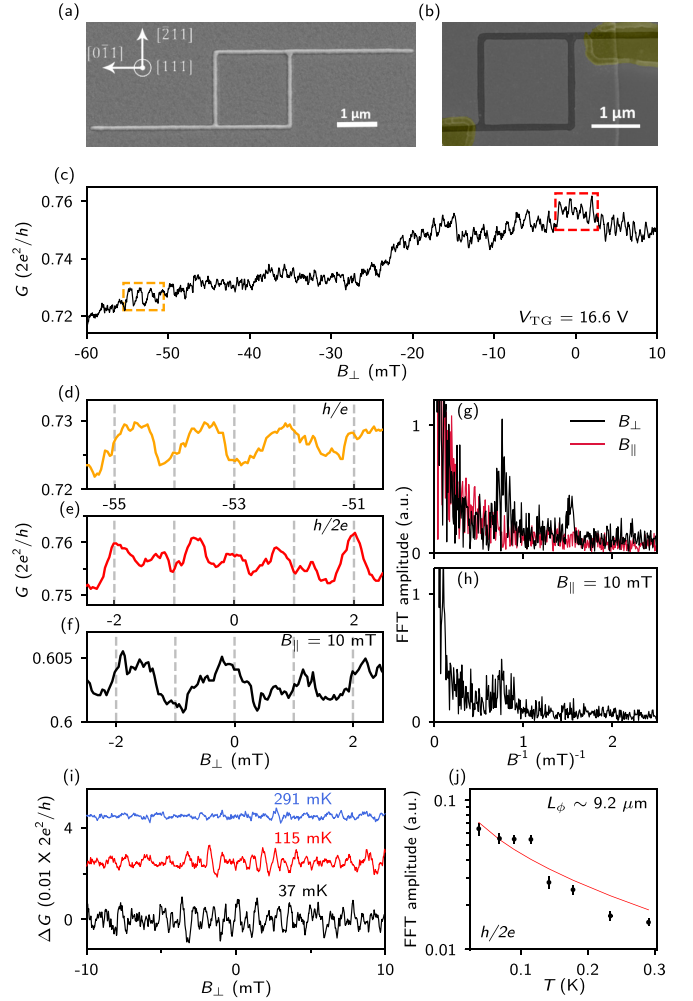


FIG. 4. AB effect in device B. (a) and (b) SEM before (a) and after (b) the fabrication of contacts (false colored yellow), dielectric, and top gate. (c) Magnetoconductance, B perpendicular to the substrate. A narrower B range is shown for clarity. Fringe temperature ~ 40 mK. (d) and (e) Magnifications of (c) (see dashed boxes), corresponding to h/e and $h/2e$ oscillations. (f) Magnification of a B scan with a fixed in-plane B of 10 mT. $V_{TG} = 16.6$ V. B offset is 5 mT for (c)–(f). (g) Black: FFT spectrum of (c). Red: FFT of a B scan (not shown) at the same gate voltage but B parallel to the substrate, serving as a control test. (h) FFT of (f) (the whole B range). (i) $h/2e$ oscillations at three different T s with background conductance subtracted. Background is smoothed over a window of 1.34 mT, close to the h/e period estimated based on the inner surface loop area. Vertical offsets are 0.025 and 0.045 $\times 2e^2/h$ for clarity. (j) T dependence of the $h/2e$ FFT amplitudes. The fitting (red line) suggests a phase coherence length ~ 9.2 μm at 50 mK.

We thank Gu Zhang and Zhan Cao for valuable discussions and Ting Lin for assistance on the TEM. This work is supported by Tsinghua University Initiative Scientific Research Program, National Natural Science Foundation of China (92065206, 51788104) and National Key Research and Development Program of China (2017YFA0303303).

- [1] A. Kitaev, Fault-tolerant quantum computation by anyons, *Ann. Phys.* **303**, 2 (2003).
- [2] C. Nayak, S. H. Simon, A. Stern, M. Freedman, and S. Das Sarma, Non-Abelian anyons and topological quantum computation, *Rev. Mod. Phys.* **80**, 1083 (2008).
- [3] L. Fu, Electron Teleportation via Majorana Bound States in a Mesoscopic Superconductor, *Phys. Rev. Lett.* **104**, 056402 (2010).
- [4] S. Plugge, A. Rasmussen, R. Egger, and K. Flensberg, Majorana box qubits, *New J. Phys.* **19**, 012001 (2017).
- [5] S. Vijay and L. Fu, Teleportation-based quantum information processing with Majorana zero modes, *Phys. Rev. B* **94**, 235446 (2016).
- [6] T. Karzig, C. Knapp, R. M. Lutchyn, P. Bonderson, M. B. Hastings, C. Nayak, J. Alicea, K. Flensberg, S. Plugge, Y. Oreg, C. M. Marcus, and M. H. Freedman, Scalable designs for quasiparticle-poisoning-protected topological quantum computation with Majorana zero modes, *Phys. Rev. B* **95**, 235305 (2017).
- [7] R. M. Lutchyn, J. D. Sau, and S. Das Sarma, Majorana Fermions and a Topological Phase Transition in Semiconductor-Superconductor Heterostructures, *Phys. Rev. Lett.* **105**, 077001 (2010).
- [8] Y. Oreg, G. Refael, and F. von Oppen, Helical Liquids and Majorana Bound States in Quantum Wires, *Phys. Rev. Lett.* **105**, 177002 (2010).
- [9] E. Prada, P. San-Jose, M. W. de Moor, A. Geresdi, E. J. Lee, J. Klinovaja, D. Loss, J. Nygård, R. Aguado, and L. P. Kouwenhoven, From Andreev to Majorana bound states in hybrid superconductor–semiconductor nanowires, *Nat. Rev. Phys.* **2**, 575 (2020).
- [10] H. Zhang, D. E. Liu, M. Wimmer, and L. P. Kouwenhoven, Next steps of quantum transport in Majorana nanowire devices, *Nat. Commun.* **10**, 5128 (2019).
- [11] V. Mourik, K. Zuo, S. M. Frolov, S. Plissard, E. P. Bakkers, and L. P. Kouwenhoven, Signatures of Majorana fermions in hybrid superconductor-semiconductor nanowire devices, *Science* **336**, 1003 (2012).
- [12] M. Deng, S. Vaitiekėnas, E. B. Hansen, J. Danon, M. Leijnse, K. Flensberg, J. Nygård, P. Krogstrup, and C. M. Marcus, Majorana bound state in a coupled quantum-dot hybrid-nanowire system, *Science* **354**, 1557 (2016).
- [13] S. M. Albrecht, A. P. Higginbotham, M. Madsen, F. Kuemmeth, T. S. Jespersen, J. Nygård, P. Krogstrup, and C. Marcus, Exponential protection of zero modes in Majorana islands, *Nature (London)* **531**, 206 (2016).
- [14] Ö. Gül, H. Zhang, J. D. Bommer, M. W. de Moor, D. Car, S. R. Plissard, E. P. Bakkers, A. Geresdi, K. Watanabe, T. Taniguchi *et al.*, Ballistic Majorana nanowire devices, *Nat. Nanotechnol.* **13**, 192 (2018).
- [15] H. Zhang, M. W. de Moor, J. D. Bommer, D. Xu, G. Wang, N. van Loo, C.-X. Liu, S. Gazibegovic, J. A. Logan, D. Car, R. L. M. Op het Veld, P. J. van Veldhoven, S. Koellinga, M. A. Verheijen, M. Pendharkar, D. J. Pennachio, B. Shojaei, J. S. Lee, C. J. Palmstrøm, E. P. Bakkers *et al.*, Large zero-bias peaks in InSb-Al hybrid semiconductor-superconductor nanowire devices, [arXiv:2101.11456](https://arxiv.org/abs/2101.11456).
- [16] H. Song, Z. Zhang, D. Pan, D. Liu, Z. Wang, Z. Cao, L. Liu, L. Wen, D. Liao, R. Zhuo, D. E. Liu, R. Shang, J. Zhao, and H. Zhang, Large zero bias peaks and dips in a four-terminal thin InAs-Al nanowire device, [arXiv:2107.08282](https://arxiv.org/abs/2107.08282).
- [17] Z. Wang, H. Song, D. Pan, Z. Zhang, W. Miao, R. Li, Z. Cao, G. Zhang, L. Liu, L. Wen, R. Zhuo, D. E. Liu, K. He, R. Shang, J. Zhao, and H. Zhang, Observation of plateau regions for zero bias peaks within 5% of the quantized conductance value $2e^2/h$, [arXiv:2205.06736](https://arxiv.org/abs/2205.06736).
- [18] S. Vaitiekėnas, A. M. Whiticar, M.-T. Deng, F. Krizek, J. E. Sestoft, C. J. Palmstrøm, S. Marti-Sanchez, J. Arbiol, P. Krogstrup, L. Casparis, and C. M. Marcus, Selective-Area-Grown Semiconductor-Superconductor Hybrids: A Basis for Topological Networks, *Phys. Rev. Lett.* **121**, 147701 (2018).
- [19] J. S. Lee, S. Choi, M. Pendharkar, D. J. Pennachio, B. Markman, M. Seas, S. Koelling, M. A. Verheijen, L. Casparis, K. D. Petersson, I. Petkovic, V. Schaller, M. J. W. Rodwell, C. M. Marcus, P. Krogstrup, L. P. Kouwenhoven, E. P. A. M. Bakkers, and C. J. Palmstrøm, Selective-area chemical beam epitaxy of in-plane InAs one-dimensional channels grown on InP(001), InP(111)B, and InP(011) surfaces, *Phys. Rev. Materials* **3**, 084606 (2019).
- [20] P. Aseev, G. Wang, L. Binci, A. Singh, S. Martí-Sánchez, M. Botifoll, L. J. Stek, A. Bordin, J. D. Watson, F. Boekhout *et al.*, Ballistic InSb nanowires and networks via metal-sown selective area growth, *Nano Lett.* **19**, 9102 (2019).
- [21] R. L. M. Op het Veld, D. Xu, V. Schaller, M. A. Verheijen, S. M. Peters, J. Jung, C. Tong, Q. Wang, M. W. de Moor, B. Hesselmann *et al.*, In-plane selective area InSb-Al nanowire quantum networks, *Commun. Phys.* **3**, 59 (2020).
- [22] G. Springholz, G. Ihninger, G. Bauer, M. Olver, J. Pastalan, S. Romaine, and B. Goldberg, Modulation doping and observation of the integral quantum Hall effect in PbTe/Pb_{1-x}Eu_xTe multi-quantum wells, *Appl. Phys. Lett.* **63**, 2908 (1993).
- [23] G. Grabecki, J. Wróbel, T. Dietl, K. Byczuk, E. Papis, E. Kamińska, A. Piotrowska, G. Springholz, M. Pinczolis, and G. Bauer, Quantum ballistic transport in constrictions of *n*-PbTe, *Phys. Rev. B* **60**, R5133 (1999).
- [24] G. Grabecki, J. Wrobel, T. Dietl, E. Papis, E. Kamińska, A. Piotrowska, A. Ratuszna, G. Springholz, and G. Bauer, Ballistic transport in PbTe-based nanostructures, *Phys. E* **20**, 236 (2004).
- [25] G. Grabecki, J. Wróbel, T. Dietl, E. Janik, M. Aleszkiewicz, E. Papis, E. Kamińska, A. Piotrowska, G. Springholz, and G. Bauer, Disorder suppression and precise conductance quantization in constrictions of PbTe quantum wells, *Phys. Rev. B* **72**, 125332 (2005).
- [26] V. A. Chitta, Jr., W. Desrat, D. Maude, B. Piot, N. Oliveira Jr, P. Rapp, A. Ueta, and E. Abramof, Integer quantum Hall effect in a PbTe quantum well, *Phys. E* **34**, 124 (2006).
- [27] G. Grabecki, J. Wróbel, T. Dietl, E. Janik, M. Aleszkiewicz, E. Papis, E. Kamińska, A. Piotrowska, G. Springholz, and G. Bauer, PbTe—A new medium for quantum ballistic devices, *Phys. E* **34**, 560 (2006).
- [28] S. G. Schellingerhout, E. J. de Jong, M. Gomanko, X. Guan, Y. Jiang, M. S. M. Hoskam, J. Jung, S. Koelling, O. Moutanabbir, M. A. Verheijen, S. M. Frolov, and E. P. A. M. Bakkers, Growth of PbTe nanowires by molecular beam epitaxy, *Mater. Quantum Technol.* **2**, 015001 (2022).
- [29] Y. Jiang, S. Yang, L. Li, W. Song, W. Miao, B. Tong, Z. Geng, Y. Gao, R. Li, F. Chen, Q. Zhang, F. Meng, L. Gu, K. Zhu, Y. Zang,

- R. Shang, Z. Cao, X. Feng, Q.-K. Xue, D. E. Liu *et al.*, Selective area epitaxy of PbTe-Pb hybrid nanowires on a lattice-matched substrate, *Phys. Rev. Materials* **6**, 034205 (2022).
- [30] Z. Cao, D. E. Liu, W.-X. He, X. Liu, K. He, and H. Zhang, Numerical study of PbTe-Pb hybrid nanowires for engineering Majorana zero modes, *Phys. Rev. B* **105**, 085424 (2022).
- [31] See Supplemental Material at <http://link.aps.org/supplemental/10.1103/PhysRevB.105.L241112> for additional data and analysis.
- [32] H. Pan and S. Das Sarma, Physical mechanisms for zero-bias conductance peaks in Majorana nanowires, *Phys. Rev. Research* **2**, 013377 (2020).
- [33] S. Das Sarma and H. Pan, Disorder-induced zero-bias peaks in Majorana nanowires, *Phys. Rev. B* **103**, 195158 (2021).
- [34] C. Zeng, G. Sharma, S. Tewari, and T. Stanescu, Partially-separated Majorana modes in a disordered medium, *Phys. Rev. B* **105**, 205122 (2022).
- [35] S. Ahn, H. Pan, B. Woods, T. D. Stanescu, and S. Das Sarma, Estimating disorder and its adverse effects in semiconductor Majorana nanowires, *Phys. Rev. Materials* **5**, 124602 (2021).
- [36] B. D. Woods, S. Das Sarma, and T. D. Stanescu, Charge-Impurity Effects in Hybrid Majorana Nanowires, *Phys. Rev. Applied* **16**, 054053 (2021).
- [37] R. A. Webb, S. Washburn, C. P. Umbach, and R. B. Laibowitz, Observation of h/e Aharonov-Bohm Oscillations in Normal-Metal Rings, *Phys. Rev. Lett.* **54**, 2696 (1985).
- [38] B. Altshuler, A. Aronov, and B. Spivak, The Aaronov-Bohm effect in disordered conductors, *Pis'ma Zh. Eksp. Teor. Fiz.* **33**, 101 (1981) [*JETP Lett.* **33**, 94 (1981)].
- [39] C. Kurdak, A. M. Chang, A. Chin, and T. Y. Chang, Quantum interference effects and spin-orbit interaction in quasi-one-dimensional wires and rings, *Phys. Rev. B* **46**, 6846 (1992).
- [40] <https://doi.org/10.5281/zenodo.6640932>.